PREPRINT UCRL-82057, Rev. 1

CONF-781245--2

Lawrence Livermore Laboratory

EVOLUTION AND EXPLOSION OF MASSIVE STARS

Thomas A. Weaver and Stanford E. Woosley

December, 1978

This paper was prepared for presentation to the 13th Texas Symposium on Relativistic Astrophysics in Munich, Germany, 14-19 December 1978.

EVOLUTION and EXPLOSION OF MASSIVE STARS*

by

Thomas A. Weaver
University of California Lawrence Livermore Laboratory
Livermore, California 94550

and

S. E. Woosley†
Board of Studies in Astronomy and Astrophysics
University of California at Santa Cruz
Santa Cruz, California 95064
and
University of California Lawrence Livermore Laboratory
Livermore, California 94550

December, 1978

* Work performed under the auspices of the U. S. Department of Energy by the UCLLL under contract number W-7405-ENG-48.

† Work performed in part under NSF contract No. AST-76-10933. Present address is University of California at Santa Cruz.

INTRODUCTION

The evolution and final fate of massive stars ($10\ M_\odot \lesssim M \lesssim 100\ M_\odot$) has long been postulated to play a central role in such important astrophysical phenomena as the origin of the chemical elements[1,2], supernova explosions[3,4], black holes[5], neutron stars[6], and cosmic rays[7]--many of which have already been the subject of vigorous discussion during this conference. In the past, these phenomena have tended to be treated separately and related to each other and to observations by idealized parameterizations that, while offering a good deal of qualitative insight into what might happen, can be criticized as isolated "fits" rather than self-consistent, quantitative explanations of such events.

This talk is mainly concerned with our attempt[8,9], within the context of current uncertainties involving supernova core physics, 2D-effects, convection, mass loss, and nuclear reaction rates, to build self-consistent evolutionary models of complete massive stars, starting from their observable zero-age main sequence configurations, and evolving through their various hydrostatic nuclear burning stages, iron core collapse, bounce, outward-going shock formation, and finally, explosive nucleosynthesis and supernova light curve formation. Previous attempts in this direction, notably by Arnett[10-15], Iben[16,17], and others[18-22], while pioneering many of the required tools and concepts, have been limited either to the early nuclear burning stages or to the treatment of simplified stellar cores. Our model[8,9] incorporates implicit hydrodynamics with a new treatment of time-dependent convection and semiconvection, and a careful treatment of the complexities of the advanced

stages of nuclear burning. This model has been used to completely evolve Population I stars of 15 and 25 $M_\odot$, with calculations for other masses and compositions in progress. We find that these models, even though they neglect mass loss, rotation, magnetic fields, and other two-dimensional effects, yield excellent agreement with the observed properties of Type II supernovae while predicting the ejection of newly created elements in the mass range from oxygen to iron (and quite possibly beyond) in ratios close to those observed in the solar system,[23] but with greatly enhanced abundances relative to hydrogen. Further, these models allow us to make a number of detailed predictions about supernova remnant abundances, γ-ray lines, supernova fluid velocities, etc., that hopefully will motivate more comprehensive observations of massive stars and supernovae.

PRESUPERNOVA EVOLUTION

Table I presents the temperatures, densities, and overall timescales that characterize the various presupernova nuclear burning stages for a 25 $M_\odot$ Population I star. It is evident that the timescales of the successive burning phases shorten dramatically, largely due to the overwhelming neutrino losses that occur at the temperatures and densities necessary to burn the higher-Z elements. As shown in Figure 1, massive stars typically begin their main sequence lives as blue giants that slowly increase in radius and luminosity as they burn hydrogen and then expand dramatically at nearly constant luminosity into blue, yellow, and finally red supergiants as they burn and exhaust helium in their cores. At this stage, about 2/3 of the star's mass resides in an envelope of nearly constant 10^{-8} g/cc density, and 10^5 °K temperature. This envelope surrounds a $\sim 3 \times 10^{10}$ cm radius mantle containing a carbon-oxygen core which rapidly contracts to a central density above 10^5 g/cc and a central temperature $\sim 7 \times 10^8$ °K, at which point carbon burning can commence. By that time neutrino losses directly from the star's core have displaced optical

radiation loss from its surface as the dominant source of energy loss that nuclear reactions must make up to keep the stars in thermal equilibrium. Indeed, the subsequent evolution takes place so rapidly compared with the thermal relaxation time of the envelope that the outward appearance of the two stars remains fixed at the positions in the H-R diagram (shown by the circled crosses in Figure 1) that they have reaced during carbon burning. Thus, unless one has a neutrino-sensitive detector, the first indication one has of the complex series of nuclear reactions that take place during the last few thousand years of the life of massive stars [and which are quite probably responsible for the production of most of the heavy ($Z \geq 8$) chemical elements now present in the universe] is when the shock wave from the collapsing, bouncing core strikes the surface resulting in the characteristic Type II supernova explosions discussed below.

The subsequent evolution of the core is the story of a complex balance between neutrino losses, degeneracy pressure, nuclear reactions, and time-dependent convection, with the core losing its battle against gravitational collapse at an ever more rapid rate as shown in Figure 2. The temporary drops in core temperatures occur when a given fuel has been exhausted in the star's center while a nuclear burning shell still remains active within the inner Chandrasekhar mass (i.e., the maximum mass of material which can support itself on degeneracy pressure alone). When the current nuclear fuel has been exhausted in this entire inner region, as well as in any exterior region to which it is joined by convective mixing, gravity overwhelms the core's residual degeneracy pressure, and it contracts and heats until the next fuel is ignited. Complex off-center burning shells also develop during neon, oxygen, and silicon burning due to composition gradients and the density dependence of the neutrino loss rate which often favors ignition at lower densities than those which occur at the innermost part of a fuel shell.

PRESUPERNOVA STRUCTURE

Figures 3 and 4 show the structure of our 25 solar mass model at a point early in iron core collapse when peak collapse velocities have nearly reached $\sim$ 1000 km/sec, and are rapidly accelerating. Additional detail and characteristics of a 15 $M_\odot$ presupernova star are given by Weaver, Zimmerman, and Woosley[8] (henceforth WZW). It is evident that the mantle of this star has evolved into an "onionskin" structure with distinct H, He, C, Ne, O, and S burning shells. These shells are typically convective, but are separated by density gradients sufficiently large to prevent convective mixing between them. Such a presupernova structure recapitulates the various evolutionary stages experienced by the star during its hydrostatic evolution, as one proceeds from the core towards the surface.

Hydrostatic silicon burning occurs over a sufficiently long timescale that the iron peak elements that result are substantially neutronized by electron capture during the burning itself. The resulting "iron" cores have masses of 1.56 $M_\odot$ and 1.61 $M_\odot$, and central electron abundances of 0.427 and 0.439 moles/g, respectively, for 15 and 25 $M_\odot$ stars. The composition is dominated by very neutron-rich species such as ^{48}Ca, ^{66}Ni, ^{54}Cr, and ^{50}Ti near the center and gradually shifts through progressively less neutron-rich species, dominated successively by ^{58}Fe, ^{56}Fe, and ^{54}Fe, as one proceeds outward. The region around Y_e=0.46 where ^{56}Fe is the dominant iron peak constituent (as it is observed to be in the solar system) covers at most a few tenths of a solar mass, while non-neutronized iron (Y_e=0.50, i.e., ^{56}Ni or ^{54}Fe + 2p), which beta decays naturally to the observed iron abundances, is present only in the narrow flashing region of the 25 $M_\odot$ star's silicon shell located at an interior mass coordinate of 1.65 $M_\odot$ (see Fig. 3). There exist discontinuities in composition and Y_e at an interior mass of approximately 1 $M_\odot$ which are fossil remnants of the outermost extent of the central convective region

during core silicon burning. Similarly, there is an abrupt fall in Y_e at the edge of the iron core corresponding to the outermost extent of the convective region associated with shell silicon burning. It is important to note that this convective mixing has allowed the iron cores to grow substantially beyond the Chandrasekhar mass ($\approx$ 1.2-1.3 $M_\odot$ for the current Y_e values) before collapse. The general character of these results appears relatively insensitive to the choice of electron-capture rates.

CORE COLLAPSE AND OUTWARD-GOING SHOCK WAVE FORMATION

It is apparent from Figure 4 that photodisintegration of the iron-peak elements to alpha particles provides the dominant source of core energy loss during the early stages of collapse. Neutrino losses due to neutronization and thermal plasma processes[24] are about a factor of 30 and 1000, respectively, less important, and the Y_e profile has not yet changed significantly from its hydrostatic value. The collapse of the iron core by these processes is a natural result of the preceding evolution and is in no way artifically induced.

These collapsing presupernova models were used as input to Wilson's detailed supernova core code [25-28], and resulted in explosions or not depending on the details of his assumptions about the physical processes taking place in the core. He and Arnett will discuss the current status of our understanding of these processes later this morning. In our present work we have sought to avoid entanglement in the very complex physics and attendant considerable uncertainties involved in current core calculations (including the probable importance of two-dimensional rotational effects), and have concentrated our attention on observable phenomena such as light curves, velocities, and nucleosynthesis which we find to be relatively insensitive to the exact manner in which the core behaves, as long as it generates a sufficiently strong outgoing shock wave to eject the mantle and envelope

($\sim 10^{51}$ ergs). Because of the widely differing response times of the core and the rest of the star, such a decoupling can be made by replacing the core with a time-dependent inner boundary condition (including an outward neutrino flux). This inner boundary condition acts like a piston which first falls in, then accelerates sharply outward to drive a shock wave into the mantle, and finally generates a rarefaction wave behind the shock as it falls back to the surface of the newly formed neutron star. Such inner boundary conditions are either taken from various (exploding) calculations of Wilson and Bowers[28] based on our initial models, or represent parameterizations of their results to give differing shock energies. Wilson will discuss examples of such calculations in the following presentation. The total explosion energies resulting for the four supernova models we will consider in this talk are given in Table 2. In each case, the explosion energies refer to the sum of all kinetic and electromagnetic (but not neutrino) energies released by the supernova.

TABLE 2: EXPLOSION ENERGIES FOR SEVERAL SUPERNOVA MODELS

MODEL	MASS ($M_\odot$)	EXPLOSION ENERGY (10^{51} erg)	MODEL	MASS ($M_\odot$)	EXPLOSION ENERGY (10^{51} erg)
15A	15	1.3	25A	25	1.4
15B	15	3.3	25D	25	4.0

Sensitivity tests in which approximately the same net energy was deposited into the mantle by differing neutrino fluxes and piston trajectories (as might occur, for example, due to different bounce densities) showed no substantial differences in nucleosynthetic yield, final velocity profiles, or photometric properties, suggesting that net explosion energy alone is a sufficiently accurate characterization of core processes for our present purposes. A possible exception to this involves the position of the mass cut, which is somewhat obscured in the present

calculation by the necessity of taking piston positions near the edge of the collapsing core where neutrino flux attenuation is small, and densities are within the range of our model. It will be argued below, however, that on the basis of nucleosynthetic, supernova light curve, and neutron star observations, the mass cut very probably occurs in the sharp density gradient near the edge of the neutronized core, as we have assumed.

EXPLOSIVE NUCLEOSYNTHESIS

The shock wave generated by the bounce of the core propagates out through the rest of the star, temporarily heating the material to temperatures sufficient to cause substantial nuclear processing in the silicon, oxygen, and neon layers just above the core. The extent of the nuclear processing which occurs is limited by the rapid, nearly adiabatic expansion of the shock-heated material, which, together with the momentum initially deposited by the shock, serves to accelerate the matter beyond its escape velocity. For the range of core explosion energies studied (1-5 x 10^{51} ergs), this shock is not particularly strong with respect to the energy density of the presupernova mantle. Indeed, shock Mach numbers of about 2 and compressions of 3-4 are typical--in contrast to the 7-fold compression which occurs in the high shock-energy limit. This circumstance implies that most of the energy in the immediately post-shock material resides as internal instead of kinetic energy. Another interesting feature of the explosion is that the density and temperature in the mantle at any given instant is roughly constant behind the shock. These characteristics allow the shock to be thought of with reasonable accuracy as an expanding bubble of radiation containing most of the energy of the core explosion. The temperature (T_s) that a given zone in the mantle reaches is then just determined by its presupernova radius (r_0) and the total internal energy (E_0) by the relation:

$$T_s(r_o) \approx \left[\frac{3E_o}{4\pi r_o^3 a}\right]^{1/4} \qquad (1)$$

where "a" is the radiation energy density constant. Peak shock temperatures are shown in Figure 5 for the weakest and strongest 25 $M_\odot$ explosions considered, and the energy/radius scaling is found to be approximately as predicted by equation (1). During the few tenths of a second for which these temperatures typically persist, material heated above $\sim 4 \times 10^9$ °K (generally initially silicon or oxygen) will be processed into non-neutronized iron peak elements[29] (predominantly radioactive ^{56}Ni) while peak temperatures between 3 and 4×10^9 °K will produce elements from silicon to calcium[29] typically from material originally rich in oxygen or neon. Peak shock temperatures between 2 and 3×10^9 °K, which mainly induce production of elements between oxygen and phosphorous, have traditionally been associated with the explosive burning of carbon.[30,31] We find, however, that the zones that reach such temperatures in our massive star models are instead composed mainly of neon and oxygen with only a trace of carbon. The zones experiencing "explosive neon burning" are particularly interesting not only because they have gone essentially unstudied to date, but also because they appear to offer an ideal site for a pre-explosive hydrostatic s-process[32], as well as for the photodisintegration-based "p"-process of Woosley and Howard[33] which produces proton-rich nucleii from s-process seed at the 2-3 billion degree temperatures characteristic of explosive neon burning. In addition, sufficient neutrons are released in the explosive burning of some neon zones to induce a limited r-process.[33,34] The mix of isotopic products from these various competing processes is a sensitive function of the peak temperature. It is thus tempting indeed to tentatively identify explosive neon burning zones as the source of many r- and p-process isotopic anomalies that have recently been observed by Wasserberg and his collaborators[35-37] in inclusions in the Allende meteorite. Further, our calculations show these

"neon" zones to contain about 1% aluminum after shock wave passage. About one part in 10^3 of this aluminum is in the form of radioactive ^{26}Al ($\tau_{1/2} = 7.3 \times 10^5$ years) whose fossil remains as an anomalous component of ^{26}Mg have also been observed in many Allende samples. While ^{26}Al is also produced in substantial quantities relative to ^{27}Al in the late phases of hydrostatic carbon burning and at the end of hydrogen burning (via the $^{25}Mg(p,\gamma)^{26}Al$ reaction)[9,38], the total mass of ^{26}Al synthesized in these latter two cases is small compared to the production in the "neon" zones.

For peak temperatures below about 2×10^9 °K, the shocked material is largely ejected without substantial explosive nuclear processing. An exception occurs at the inner edge of the helium shell where peak temperatures in the vicinity of 10^9 °K and densities near 10^4 g cm^{-3} are sufficient to generate an intense neutron pulse that lasts for about half a second (see Figure 6). This flux is sufficient to drive a "mini-r" process[39,40] that shifts iron-peak isotopes upwards by several mass units and produces even heavier r-process elements from the enhanced s-process seed already present in the region. While the details of this process are currently being worked out in collaboration Blake and Schramm[41], it appears possible to produce substantial amounts of r-process isotopes having masses between 56 and 80 by this process. Such isotopes tend to be underproduced in the higher neutron flux conditions required for the classical (as yet siteless) r-process that produces heavier isotopes.[42]

Judgment of any nucleosynthetic study must ultimately rest on how well the overall ratios of elements and isotopes it produces reproduce the observed solar abundances when averaged over a suitable distribution of objects. The final composition profiles of the ejected ashes of 15 and 25 $M_\odot$ stars are shown in Figure 7, and are to be compared to the presupernova composition profiles given in Figure 3 and WZW. It is apparent that explosive processing is primarily responsible for the elements between silicon and iron, while those from oxygen

to magnesium are formed hydrostatically and have abundances largely unmodified by explosive ejection. It is also evident that 25 $M_\odot$ stars produce about a factor of 5 greater mass per star of $Z > 2$ ashes than do 15 $M_\odot$ stars. Indeed, the mass fraction, Z_{ej}, of the high -Z ashes in stars we have studied in the 15-50 $M_\odot$ range can be well fit by the function:

$$Z_{ej} \approx 0.5 - \frac{6.3}{M} \qquad (2)$$

where M is the mass of the star in solar masses. When this fraction of high -Z products is multiplied by the stellar birth rate as a function of mass as compiled by Scalo and Miller[43], the resulting curve (shown in Fig. 8) indicates the relative average contribution to nucleosynthesis of stars in a given mass range (see also references 44-46). While this curve peaks at 18.5 $M_\odot$ its median value is 29 $M_\odot$, a number fairly insensitive to the choice of upper mass cut-off. Roughly speaking then, one might expect a star of about 25 $M_\odot$ to be a "typical nucleosynthetic object" (at least among massive stars which undergo iron-core-collapse-induced supernova explosions). Thus it is very pleasing that the elements in the mass range between oxygen* and iron that are produced and ejected by the 25 $M_\odot$ supernova are enhanced by a large and almost uniform factor of 25 relative to hydrogen, within the factor-of-two errors in the solar abundance determinations[23] (as shown in Figure 9(a)). Indeed, the solar abundance of Ne, the most discrepant element, is difficult to determine experimentally. Recent planetary nebulae observations by Kaler[47] suggest a value 50% higher than Cameron[23] gives for the solar system. This would have the effect of lowering the points shown for Ne in Fig. 9(a) by 50%, bringing it into excellent agreement with the other elements. As expected, the overall enhancement factors for the 15 $M_\odot$ star shown in Fig. 9(b) bear considerably

* Note that carbon and nitrogen are expected to be produced copiously in lower mass stars[49], so that their underproduction here does not pose a problem.

less resemblance to the solar abundances, and that star is found to be dominantly enhanced in neon, magnesium, and silicon. Note, however, that many elemental ratios in the 15 $M_\odot$ star are still quite close to their solar values.

These figures also serve to demonstrate that the energy of a supernova explosion has relatively little effect on its net nucleosynthetic yield. The main effect of increased energy is to shift the regions experiencing explosive neon and oxygen burning outward in the star while leaving their total masses relatively unchanged, resulting in more neon burnup, increased iron production, and other small changes. This nucleosynthetic insensitivity to explosion energy is quite reassuring in the face of our uncertain understanding of the complex supernova core physics.

TYPE II SUPERNOVA LIGHT CURVES

Representative electromagnetic displays produced by our two 15 $M_\odot$ supernova models are shown in Figure 10, compared to photometric data for Supernova 1969ℓ in NGC 1058, perhaps the best observed Type II supernova.[49-50] SN 1969ℓ is characteristic of a common subclass of Type II supernovae which shows a 2-3 month initial plateau in its visual emission ($M_V \approx -17$) followed by a rapid decline of about 2 stellar magnitudes and then a slower decline at a rate of $\sim$ 3 magnitudes/year. (SN 1970g in NGC 5457 = M101 is another recent example of this subclass).[51] It is apparent that the theoretical and observational results are in excellent agreement. As Figure 10 shows, an increase in the energy of the core explosion produces a roughly linear increase in the optical brightness together with a shorter "plateau." Although we have chosen to focus our comparison on 15 $M_\odot$ supernovae which are expected to occur more frequently,[43] the results for our 25 $M_\odot$ models are generally quite similar (see Weaver and Woosley[9]). Note in particular that this agreement has not been achieved by normalizing the observational absolute magnitude so as to provide the best fit.

Figures 11 and 12 compare derived observational SN 1969ℓ results[49,50,52] for the temperature and radius of the supernova photosphere with the corresponding theoretical results. Figure 13 shows a comparison between observed absorption line velocities and photospheric velocities for the low energy 15 $M_\odot$ explosion. The agreement between theory and observation is uniformly within the observational errors, and allows a confident description of the general physical processes which are occurring (see also references 14, 15, and 53 for conclusions based on parameterized models).

The initial sharp spike in temperature and luminosity at small photospheric radius corresponds to the breakout of the supernova shock through the surface of the star's supergiant envelope. This is accompanied in theory[9,54] by a $\sim$ 2000 sec long, soft X-ray pulse with an equivalent black body temperature $\sim 1.5 \times 10^5$ °K and a peak luminosity $\sim 10^{45}$ erg/sec. The surface is then rapidly cooled by radiative emission and hydrodynamic expansion, balanced in part by radiative diffusion from below. The photosphere expands rapidly in physical size, but slowly recedes with respect to the envelope material as the optical thickness of that material decreases due to rarefaction. After about 20 days, the photosphere has cooled to roughly 6000 °K, the temperature at which hydrogen recombines at the extremely low densities ($\sim 10^{-13}$ g/cc) prevalent in the envelope. Over the next 2 months or so, a transparency wave eats its way into the envelope with the photospheric temperature remaining near 6000 °K (see Figures 11-12). In doing so, material traveling at lower and lower velocities is uncovered until the speed of the cooling wave exceeds the fluid velocity, and the photosphere physically recedes until it encounters the slowly moving (< 100 km/sec), relatively dense, and very optically thick mantle. At this point a transient increase in the photospheric temperature occurs and persists for $\sim$ 2-3 days due to the uncovering and rapid cooling of the hot surface of the mantle. This phenomenon is potentially observable, although non-LTE radiation

effects in the overlying envelope may tend to mask it. The sharpness of this final recession and the resulting fall in luminosity is probably artificially abrupt due to our relatively simplified treatment of recombination and non-LTE radiation effects.

At late times the luminosity is due to thermalized radiation from the decay of the explosively generated* ^{56}Ni ($\tau_{1/2}$ = 6.1 days) and its daughter ^{56}Co ($\tau_{1/2}$ = 78.5 days) diffusing out of the mantle. As the figures show, models with ^{56}Ni decay turned off display a much more sharply falling luminosity tail as the residual thermal energy in the mantle diffuses out over a characteristic time of only 1-2 months. In models containing energy input from radioactivity the convolution of radiation escape and ^{56}Co decay times produces a luminosity decline slower than the 78-day ^{56}Co half-life, particularly in the 25 $M_\odot$ case. [Indeed it is tempting to speculate that all supernova tails are due at late times to ^{56}Co decay with the apparent decay time either shortened by incomplete absorption of the decay γ-rays (e.g. Type I supernova) or lengthened by the temporary trapping of the thermalized decay energy by an optically-thick envelope. (See reference 55 for related models.)] The ripples in the theoretical curves at late times are due to the (possibly numerical) formation of density clumps (see Fig. 14 and reference 56) in the mantle (which appear to offer excellent sites for grain formation). It is likely two-dimensional instabilities will also occur[57] (as is suggested by observations of supernova remnants) which should have the effect of increasing the noise, but damping the size of transient excusions in the luminosity.

Useful information about supernova models can be obtained from their light curves. At early times ($\lesssim$ 3 months) the light curve principally conveys information about the structure of the envelope of the presupernova star. More

* The mass of ^{56}Ni produced during explosive silicon burning is 0.08, 0.12, 0.36 and 0.43 $M_\odot$ in models 15A, 15B, 25A, and 25D, respectively.

massive, extended envelopes produce prolonged luminosity plateaus and slower photospheric velocities for fixed shock energies. The behavior of the tail of the light curve, on the other hand, yields information about the size and density of the mantle and, potentially, its composition. The deduced amount of ^{56}Ni may serve to indicate the position of the mass-cut between the core and the mantle for a star of given mass. Additional information comes from γ-ray lines resulting from the decay of ^{56}Co and perhaps ^{60}Co in young supernovae placed in nearby galaxies. The observed flux is critically dependent on the time at which the mantle becomes transparent to γ-rays and thus on its density profile and fluid velocities. Detailed predictions of γ-ray line strengths and profiles are currently being calculated by Axelrod (at LLL)[58] based on our supernova models, and should be complete before the launch of HEAO-C.

SUPERNOVA REMNANT MASS

The above results have direct implications for the masses of the neutron star or black hole remnants likely to result from massive star evolution. In particular, as was pointed out by WZW[8], the neutronized iron cores that form in these stars contain such large quantities of ^{54}Fe and rare highly neutronized iron peak species that at most $\sim 0.03\ M_\odot$ of the core's mass can be ejected on the average if massive overproduction of these isotopes is to be avoided. Further, our explanation for Type II supernova light curves suggests that the 0.1-0.4 $M_\odot$ of explosively generated ^{56}Ni which lies directly above the neutronized core must be at least partly ejected in order to provide the energy to produce late-time light curve tails. While additional stellar models and light curve observations are obviously needed to clarify the statistics and generality of these conclusions, the direct implication is that the initial mass of a condensed supernova renmant should fall within 0.1-0.2 $M_\odot$ of the mass of the presupernova iron core. (1.56 and 1.61 $M_\odot$, respectively, for our 15 and 25 $M_\odot$ models.) The mass cut thus falls quite plausibly in the steep density gradient occurring at the edge of the core, and indeed most of the calculations of

Wilson[25-28] that lead to $\sim 10^{51}$ erg explosions exhibit such behavior. Allowing for the 10% mass decrease due to neutrino emission, the corresponding observable neutron star remnant masses would be 1.40 and 1.45 $M_\odot$, respectively. These masses are in excellent agreement with the precisely measured masses of the components of the binary pulsar 1913 + 16 as reported by Taylor[59] to be 1.39 ± 0.15 and 1.44 ± 0.15 $M_\odot$, and with other less accurate observations of neutron star masses[60].

CONCLUSIONS and NEED FOR FUTURE WORK

Despite the remarkable agreement of our theoretical supernova models with the relatively sparse available data for Type II explosions, it would be erroneous to assume that we now understand such phenomena in their entirety. Instead, we would hope that the detailed predictions which come out of these models concerning such quantities as photospheric temperature, velocity, radius, and luminosity as a function of time; abundances in supernova remnants and in the galaxy; and γ-line fluxes will aid in justifying (and help provide a basis for interpreting) further extensive observations of supernovae and highly evolved massive stars. The excellent supernova search and observation program at Asiago[61] provides a promising start in this direction and deserves support. Frequent multifrequency scans of known supernovae when used in conjunction with our temperature and density predictions and taking non-LTE effects into account should yield good abundance data not only for the surfaces of these stars, but also for the underlying layers. Another exciting application of such extensive observations is that when combined with further refinements in the theory of supernova atmospheres they should allow the accurate use of supernova as both standard[61] and "non-standard"[15,62] candles for determining distances to distant galaxies. Computerized sky searches of the kind pioneered by Colgate[63] would also be quite valuable in discovering supernovae in an early enough phase to study shock break-out and to uniformly calibrate light curves at early times. The importance of detecting and analyzing the predicted γ-lines from young ($\sim$ 1

year old) supernova remnants cannot be overstated. Data from the ^{56}Co decays will yield valuable information about the interior of supernovae and the "mass cut" as well as directly confirming in the strongest possible way the existence of explosive nucleosynthesis. We look forward to HEAO-C (or a galactic supernova).

On the theoretical front, we cannot claim a true understanding of supernovae until such (real) complications as mass loss, Raleigh-Taylor instabilities, rotation, magnetic fields, and uncertainties in convection theory have been properly addressed. This may not occur in our lifetimes! In the more immediate future we see as requisite extensions of our own (benchmark) work the consideration of stars of other masses and populations (only Population I 15 $M_\odot$ and 25 $M_\odot$ stars have been treated here) and extensive non-LTE studies of the emission/absorption features of the photospheres in our models (hopefully to be performed by others). The evolution and possibly explosive demise of stars with $M < 10\ M_\odot$ and $M > 100\ M_\odot$ deserves careful attention and may ultimately prove to be important nucleosynthetic sites. The collapsing cores of stars in the range $10 \lesssim M/M_\odot \lesssim 100$ obviously need further study. By treating the core bounce as a simple inner boundary condition we have temporarily averted a confrontation with the uncertainties that accompany the study of neutrino physics and the equation of state for matter at (super-) nuclear density. While we have not addressed the core-bounce problem it is at least reassuring that the bulk of observed (and observable) supernova properties do not appear to be especially sensitive to the precise manner in which energy is coupled into the mantle and envelope providing, of course, as we apparently have been repeatedly assured by nature, that the cores of these stars do in fact blow up!

ACKNOWLEDGMENTS

We gratefully acknowledge the use of unpublished supernova core models of J. R. Wilson and R. L. Bowers, as well as the encouragement and support of Lowell Wood and Edward Teller. We have profited by numerous private conversations with many researchers in the fields of supernova dynamics, nucleosynthesis, and observations. Chief among this group (whose names must be omitted for lack of considerable

space) are W. A. Fowler and W. D. Arnett who, by both suggestion and example, have served to motivate much of this work.

REFERENCES

1. Hoyle, F. 1946. MNRAS, 106: 343.
2. Burbidge, E.M. Burbidge, G. R., Fowler, W. A., and Hoyle, F. 1957, Rev. Mod. Phys. 29: 547.
3. Colgate, S. A., and White, R. H. 1966. Ap. J. 146: 626.
4. Fowler, W. A., and Hoyle, F. 1964. Ap. J. Suppl. No. 91, 9: 201.
5. Oppenheimer, J. R., and Volkoff, G. M. 1939. Phys. Rev. 55: 374.
   Zeldovitch, Ya. B. 1964. Soviet Phys. - Dokl. 9: 195.
6. Oppenheimer, J. R., and Snyder, H. 1939. Phys. Rev. 56: 455.
   Penrose, R. 1969. Riv. Nuovo Cim., Numero Speciale 1: 252.
7. Colgate, S. A. 1969. In Proc. 11th Intern. Conf. Cosmic Rays (Budapest: Akademia: Kiado).
   Colgate, S. A., and Johnson, M. H. 1960. Phys. Rev. Letters 5: 235.
8. Weaver, T. A., Zimmerman, G. B., and Woosley, S. E. 1978. Ap. J. 225: 1021.
9. Weaver, T. A. and Woosley, S. E. 1979, in preparation.
10. Arnett, W. D. 1969. Astrophys. Space Sci. 5: 180.
11. _____. 1972. Ap. J. 176: 681, 176: 699; 173: 393.
    _____. 1973. Ap. J. 179: 249.
12. _____. 1974. Ap. J. 193: 169; 194: 373.
    _____. 1977. Ap. J. Suppl. 35, 145.
13. _____. 1978. Ap. J. 219: 1008.
14. Falk, S. W., and Arnett, W. D. 1973. Ap. J. (Letters) 180: L65.
    _____. Ap. J. Suppl. 33: 515.
    Arnett, W. D., and Falk, S. W. 1976. Ap. J. 210: 733.
15. Schurmann, S. R., Arnett, W. D., and Falk, S. W. 1978. Preprint.
16. Iben, I. 1975. Ap. J., 196: 525.
17. Lamb, S. A., Iben, I., and Howard, W. M. 1976. Ap. J., 207: 209.
18. Barkat, Z. 1971. Ap. J., 163: 433.
19. Ikeuchi, S., Nakazawa, K., Murai, T., Hoshi, R., and Hayashi, C. 1971. Prog. Theor. Phys., 46: 1713; and 1972. ibid., 48:1870.

20. Encal, A. S. 1975. Ap. J., 195: 187 and 197: 405.

21. Sugimoto, D. 1970. Prog. Theor. Phys., 44: 599; see also 1971. ibid., 45: 461.

22. Rakavy, G., Shaviv, G., and Zinamon, Z. 1967. Ap. J., 150: 131.

23. Cameron, A. G. W., 1973, in Explosive Nucleosynthesis, ed. D. N. Schramm (University of Texas Press: Austin).

24. Beaudet, G., Petrosian, V., and Salpeter, E. E. 1967. Ap. J., 150: 979.

25. Wilson, J. R. 1971. Ap. J., 163: 209.

26. _____. 1974. Phys. Rev. Lettr., 32: 849.

27. _____. 1977. Varrena Lectures, to be published.

28. Wilson, J. R., and Bowers, R. L. 1978. Private communication; Wilson, J. R. 1978, this conference.

29. Woosley, S. E., Arnett, W. D., and Clayton, D. D., 1973. Ap. J. Suppl. No. 231, 26: 231.

30. Arnett, W. D. and Truran, J. W., 1969. Ap. J., 157: 339.

31. Pardo, R. C., Couch, R. G., and Arnett, W. D., 1974. Ap. J., 191: 711.

32. Lamb, S. A., Howard, W. M. Truran, J. W., and Iben, I. 1977. Ap. J., 217: 213.

33. Woosley, S. E., and Howard, W. M., 1978. Ap. J. Suppl., 36: 285.

34. Howard, W. M., Arnett, W. D. Clayton, D. D., and Woosley, S. E., 1972. Ap. J., 175: 201.

35. Lee, T., Papanastassiou, D. A., and Wasserburg, G. J., 1977. Ap. J. Lettr., 211: L107.

36. _____. 1978. Ap. J. Lettr., 220: L15.

37. McCulloch, M. T., and Wasserburg, G. J., 1978. Ap. J. Lettr., 220: L15; see also Geophys. Res. Lettr., 5: 599.

38. Woosley, S. E., and Weaver, T. A., 1979. In preparation.

39. Truran, J. W., Cowan, J. J., and Cameron, A. G. W., 1978. Ap. J. Lettr., 222: L63.

40. Thielemann, F. K., Arnould, M., and Hillebrandt, W., 1978. Submitted to Astron. and Ap.

41. Blake, B. T., and Schramm, D. N., 1978. Private communication.

42. Seeger, P. A., Fowler, W. A., and Clayton, D. D., 1965. Ap. J. Suppl. No. 97, 11: 121.

43. Miller, G. E., and Scalo, J. M., 1979. Preprint.

44. Arnett, W. D., and Schramm, D. N., 1973. Ap. J., 184: L47.

45. Talbot, R. J., and Arnett, W. D., 1973. Ap. J., 186: 51.

46. Ostriker, J. P., Richstone, D. O., and Thuan, T. X., 1974. Ap. J., 188: L87.

47. Kaler, J. B., 1978. Ap. J., 225: 527.

48. Shields, G. A., 1978. Ap. J., 219: 559 and 565.
Farland, G. J. and Shields, G. A., Ap. J., 226: 172.

49. Ciatti, F., L. Rosino, and F. Bertola. 1971. Mem. Soc. Astron. Ital. 42: 163.

50. Kirshner, R. P., Oke, J. B., Penston, M. V., and Searle, L. 1973. Ap. J. 185: 303, and references cited therein.

51. Barbon, R., Ciatti, F., and Rosino, L. 1973. Astron. & Astrophys. 29: 57.

52. Kirshner, R. P., and J. Kwan. 1974. Ap. J. 193: 27.

53. Chevalier, R. A. 1976. Ap. J. 207: 872.

54. Lasher, G. J., and K. L. Chan. 1978. Preprint.
See also Klein, R. I., and Chevalier, R. A. 1978. Ap. J. (Letters) 223: L109.

55. Colgate, S. A. and McKee, C. 1969. Ap. J. 157: 623.

56. Isenberg, P. A. 1977. Ap. J. 217: 597.

57. Chevalier, R. A. and R. I. Klein. 1978. Ap. J. 219: 931.

58. Axelrod, T. S. 1979. Ph.D. Thesis, in preparation.

59. Taylor, J. H. 1978, this conference.

60. Lewin, W. H. G. 1978, this conference; Bahcall, J. N. 1978. Ann. Rev. Astron. Astrophys. 16: 241.

61. Rosino, L. 1977. In Supernovae, D. N. Schramm (ed.), (Dordrecht-Holland: Reidel).
Rosino, L. and G. Di Tullio. 1974. In Supernovae and Supernova Remnants, C. B. Cosmovici (ed.), (Dordrecht-Holland: Reidel).

62. Branch, D. 1977. In Supernovae, D. N. Schramm (ed.), (Dordrecht-Holland: Reidel)

63. Colgate, S. A., E. P. Moore, and R. Carlson. 1975. Pub. A. S. P. 87: 565.
Colgate, S. A., E. P. Moore, and J. Colburn. 1975. Applied Optics 14: 1429.

TABLE I

NUCLEAR BURNING STAGES

25 $M_\odot$ STAR

BURNING STAGE	TEMPERATURE	DENSITY	TIMESCALE
Hydrogen	5 keV	5 g/cc	7×10^6 years
Helium	20 keV	700 g/cc	5×10^5 years
Carbon	80 keV	2×10^5 g/cc	600 years
Neon	150 keV	4×10^6 g/cc	1 year
Oxygen	200 keV	10^7 g/cc	6 months
Silicon	350 keV	3×10^7 g/cc	1 day
Collapse	600 keV	3×10^9 g/cc	Seconds
Bounce	3 MeV	10^{13} g/cc	Milliseconds
Explosive	200-600 keV	Varies	.1 - 100 Seconds

FIGURE CAPTIONS

Figure 1 Evolutionary paths of the present 15 $M_\odot$ and 25 $M_\odot$ model stars in the H-R diagram (diamonds) compared with the reuslts of Lamb, Iben, and Howard[17] (solid lines). Virtually all of the evolutionary motion of these stars in the H-R diagram occurs before the onset of core carbon burning. The final post-carbon-burning (i.e., presupernova) location is shown as a circled cross for each present stellar model.

Figure 2 Thermodynamic history of the center of a 25 $M_\odot$ Population I star during carbon, neon, and oxygen burning. Burning characteristics and elapsed time spent during each phase are given along the evolutionary path and the dramatic increase in the star's total neutrino luminosity (L_ν) during these phases is noted. "Off-center" shell burning, in which the contracting shell of nuclear fuel first ignites at a location outward of its inner boundary due to the large density dependence of the neutrino losses, is a common occurrence as shown. This results in temperature and composition inversions that are typically transient.

Figure 3 Presupernova composition profile of a 25 $M_\odot$ Population I star as a function of the interior mass coordinate as given by WZW[8]. The structure is shown at the point at which collapse velocities in the iron core have nearly reached 1000 km/sec and are rapidly increasing. In the region interior to the 1.61 $M_\odot$ where a 131-isotope quasi-equilibrium nuclear burning network was used to treat quasistatic silicon burning and neutronization, the curve labeled "^{56}Ni" includes minor contributions from other $A \approx 2Z$ iron peak nucleii; the curve

labeled "^{54}Fe" includes those iron peak isotopes with $A \approx 2(Z+1)$, while that labeled "Fe" includes all other isotopes with $Z \geq 22$ (e.g., ^{56}Fe, ^{58}Fe, and major contributions from highly neutronized iron peak species such as ^{48}Ca, ^{66}Ni, ^{50}Ti, etc.). For additional details and a similar plot for a 15 $M_\odot$ star, see WZW[8].

Figure 4 The thermodynamic structure of the presupernova 25 $M_\odot$ model star described in Fig. 3 is shown as a function of mass fraction. Note that the density and temperature profiles are plotted such that the curves will maintain constant separation for the case $\rho \propto T^3$. Here $-\dot{S}_T$ is the total local energy loss rate due to both neutrino emission and nuclear photodisintegration, $\dot{S}_\nu$ is the total neutrino energy loss rate, and $\dot{S}_{\nu p}$ is the neutrino energy loss rate due to the thermal plasma processes. The nuclear energy generation rate profiles for the various nuclear burning shells are labeled $\dot{S}_N$, and the principal nuclear fuel is indicated. All energy generation and loss rates share the common scale denoted by "S." Active convective regions are indicated by striped bars, while semi-convective and convectively neutral regions are shown as outlined bars. In this figure, R, T_{eff}, and L denote the photospheric radius, effective temperature, and optical luminosity, respectively. For additional details and a similar plot for a 15 $M_\odot$ star, see WZW[8].

Figure 5 Peak explosion temperatures as a function of mass fraction and pre-explosion composition for the 25 $M_\odot$ model supernovae given in Table II. The peak temperature experienced in each zone scales roughly as the fourth root of the explosion energy as is expected from the simple radiation dominated model described in the text.

Substantial explosive burning of neon, oxygen, and silicon are expected to occur but a significant amount of hydrogen, helium, or carbon burning appears unlikely.

Figure 6 Thermodynamic conditions and neutron flux experienced by the helium burning shell during the supernova explosion of a 15 $M_\odot$ star. Time is measured relative to the time of shock wave passage. The initial composition of this zone contained 4.5% ^4He and 1.2% ^{22}Ne by mass with the remainder in the form of ^{12}C, ^{16}O, and a distribution of heavier elements resulting from a pre-explosive s-process. These explosion characteristics will lead to a limited form of r-process. The total neutron fluence is insensitive to the ρ and T_9 risetime during shock (which is here artificially slow due to the use of artificial viscosity to mediate the shock).

Figure 7 The final elemental composition of the 15 $M_\odot$ (Fig 8a) and 25 $M_\odot$ (Fig. 8b) post-supernova models having explosion energies of 1.3×10^{51} ergs (Model 15A) and 1.4×10^{51} ergs (Model 25A), respectively, is shown as a function of the interior mass coordinate. The term "neutronized core" refers to material which contains such large concentrations of rare neutron-rich isotopes (e.g., ^{58}Fe, ^{48}Ca) that only a small fraction could, on the average, be ejected into the interstellar medium. For mass zones exterior to those shown in the Figure, the pre-explosive composition (ashes of hydrostatic burning phases) is ejected into the interstellar medium virtually unmodified.

FIGURE CAPTIONS (Continued)

Figure 8 The product of the Miller-Scalo[43] stellar birth function and the Weaver-Woosley[9] supernova yield function as a function of stellar mass.

Figure 9 The enhancement factor, defined as the mass of an element in all material external to the neutronized core divided by the mass of hydrogen and normalized to a similar ratio in the solar system[23], is given as a function of mass for 15 $M_\odot$ (Fig. 9a) and 25 $M_\odot$ (Fig. 9b) Pop. I supernovae. Black circles represent enhancement factors in the pre-supernova star at the time of core collapse. Open squares and triangles represent the nucleosynthesis of relatively low energy (15A, 25A) and high energy explosions (15B, 25D), respectively.

Figure 10 Light curve of Type II supernova 1969ℓ compared to 15 $M_\odot$ theoretical models. Here, M_b is the absolute bolometric magnitude of the supernova and time is measured with respect to core bounce for the theoretical models and Julian day 2,440,560 for the observations. The solid and dotted lines give the bolometric luminosity for Models 15A and 15B, while the data points for 1969ℓ are either derived from the UBV data of Ciatti, et al.[49] as transformed by the method of Schurmann, et al.[15] (open circles) or obtained by integrating the multifrequency scans of Kirshner et al.[50] (open squares). The dot-dashed curve shows the result when ^{56}Ni decay is artificially suppressed in Model 15A.

Figure 11 Photospheric temperature of Type II supernova 1969ℓ compared with 15 $M_\odot$ theoretical models. The solid and dotted lines give the results for Models 15A and 15B, while the solid circle data points represent the data of Ciatti,et al.[49] as transformed by Kirshner and Kwan.[52] The open circle data points are obtained by extrapolating the transformation

FIGURE CAPTIONS (Continued)

Figure 11 (Cont'd) methods of Kirshner and Kwan[52] to the late time data of Ciatti, et al.[49], and are associated with "?" marks where lines dominate the spectrum and such color/temperature transformations become dubious. The open triangle data points are derived from fits to multifrequency scans.[50]

Figure 12 Photospheric radius of Type II supernova 1969 compared to 15 $M_\odot$ theoretical models. Solid and dotted lines give the results for Models 15A and 15B, while the 1969ℓ data points are either derived from UBV data[49] or multifrequency scans.[50]

Figure 13 Surface and photospheric velocities as a function of time from Model 15A compared with absorption lines velocities observed for supernova 1969ℓ.[50]

Figure 14 Density, temperature, and pressure plotted as a function of interior mass for Model 15A at a time since core bounce (7.12×10^7 sec) when conditions for grain formation in the mantle appear most favorable.

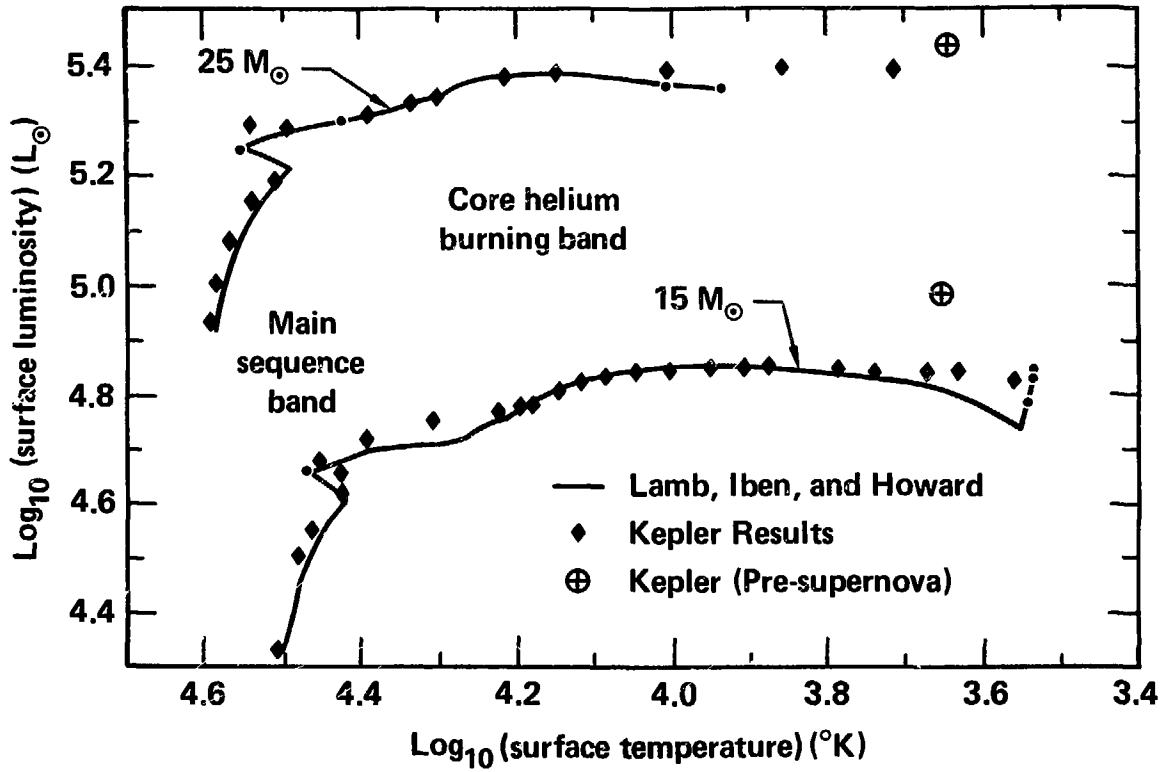
25 M⊙
15 M⊙
Core helium
burning band
Main
sequence
band
Lamb, Iben, and Howard
Kepler Results
Kepler (Pre-supernova)
5.4
5.2
5.0
4.8
4.6
4.4
4.6
4.4
4.2
4.0
3.8
3.6
3.4
Log10 (surface luminosity) (L⊙)
Log10 (surface temperature) (°K)

FIGURE 1

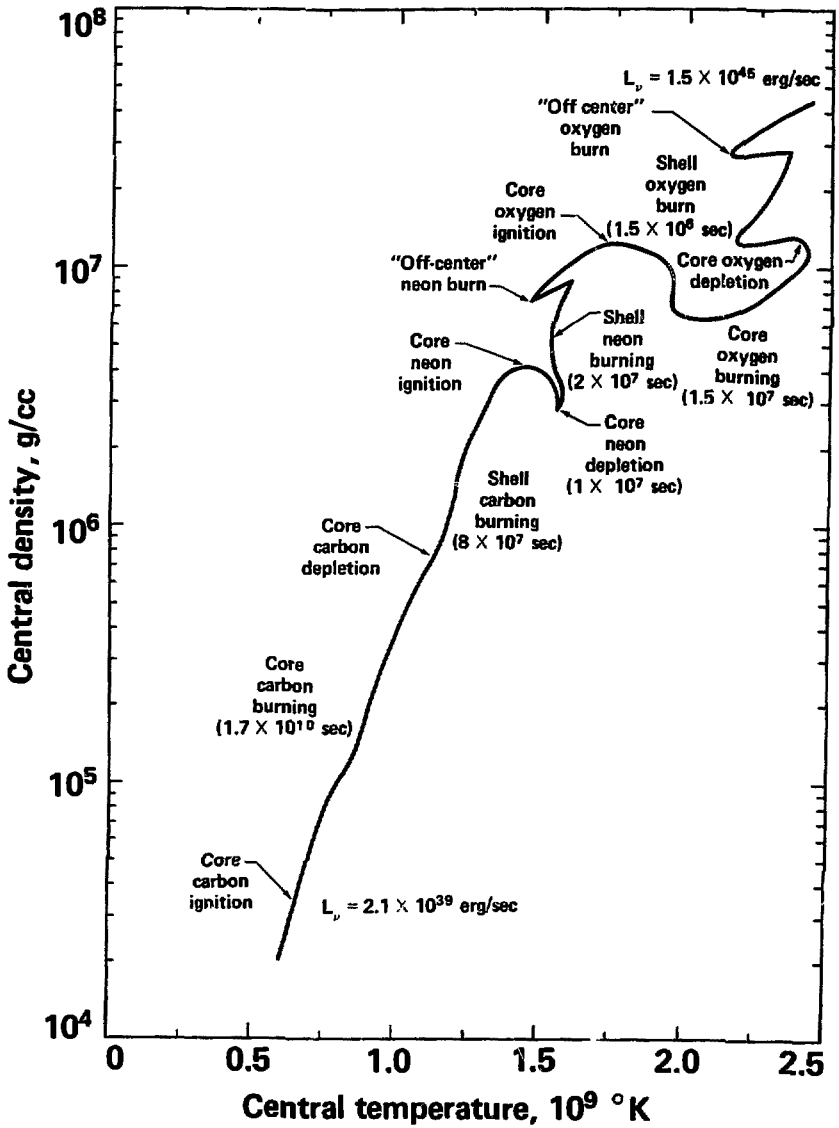
10^8
10^7
10^6
10^5
10^4
Central density, g/cc
0
0.5
1.0
1.5
2.0
2.5
Central temperature, 10^9 °K
L_ν = 1.5 X 10^{45} erg/sec
"Off center" oxygen burn
Shell oxygen burn (1.5 X 10^8 sec)
Core oxygen ignition
"Off-center" neon burn
Core oxygen depletion
Shell neon burning (2 X 10^7 sec)
Core neon ignition
Core oxygen burning (1.5 X 10^7 sec)
Core neon depletion (1 X 10^7 sec)
Shell carbon burning (8 X 10^7 sec)
Core carbon depletion
Core carbon burning (1.7 X 10^{10} sec)
Core carbon ignition
L_ν = 2.1 X 10^{39} erg/sec

FIGURE 2

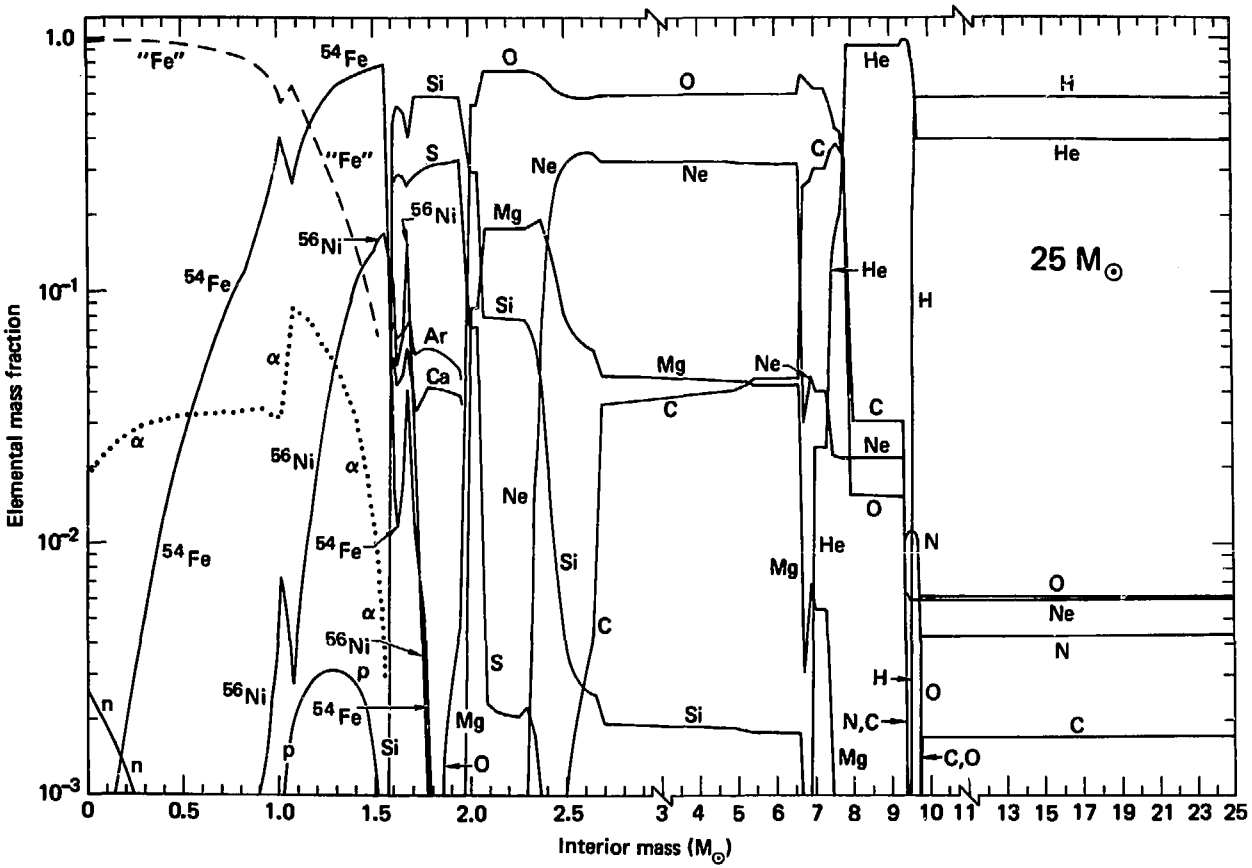
Elemental mass fraction
Interior mass ($M_\odot$)
25 $M_\odot$
"Fe"
^{54}Fe
^{56}Ni
α
n
p
Si
S
Ar
Ca
Mg
Ne
O
C
N
H
He

FIGURE 3

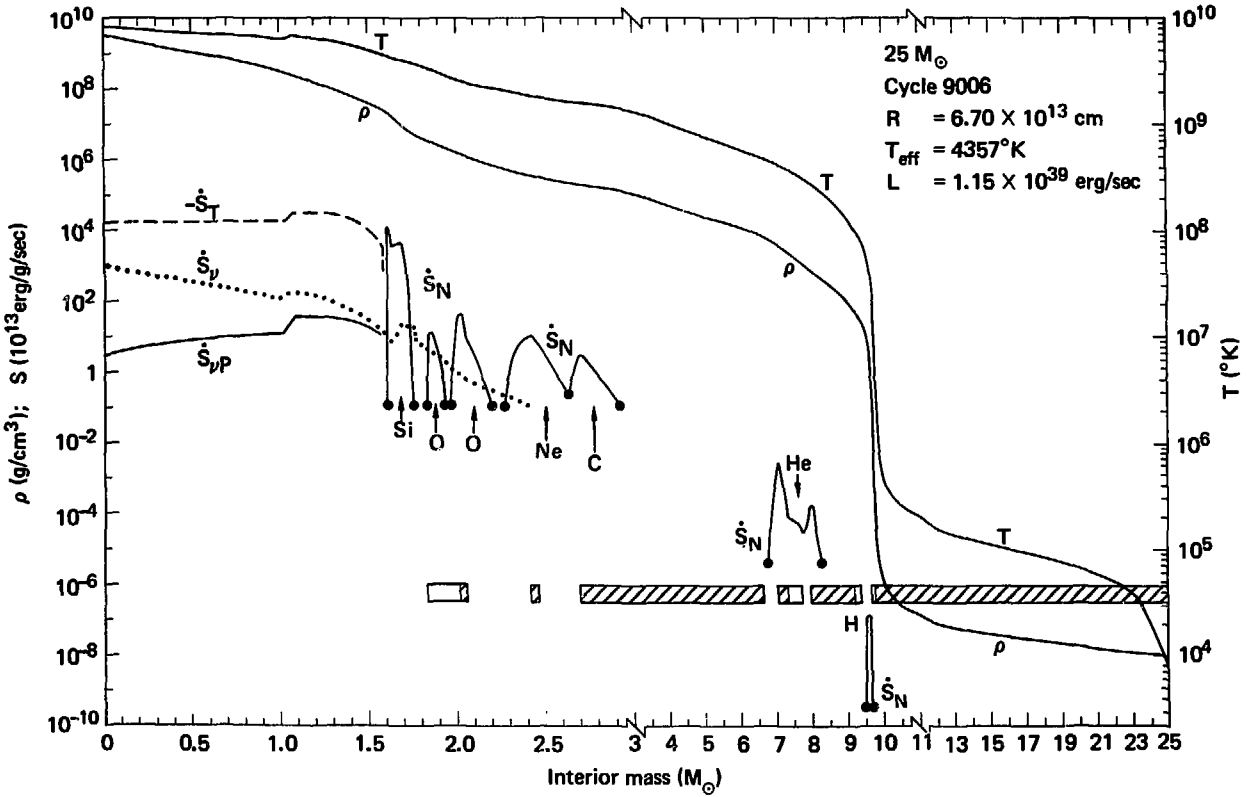
25 M⊙
Cycle 9006
R = 6.70 X 10^13 cm
T_eff = 4357°K
L = 1.15 X 10^39 erg/sec
T
ρ
-Ṡ_T
Ṡ_ν
Ṡ_νP
Ṡ_N
Si
O
O
Ne
C
He
H
ρ (g/cm^3); S (10^13 erg/g/sec)
T (°K)
Interior mass (M⊙)
0 0.5 1.0 1.5 2.0 2.5 3 4 5 6 7 8 9 10 11 13 15 17 19 21 23 25

FIGURE 4

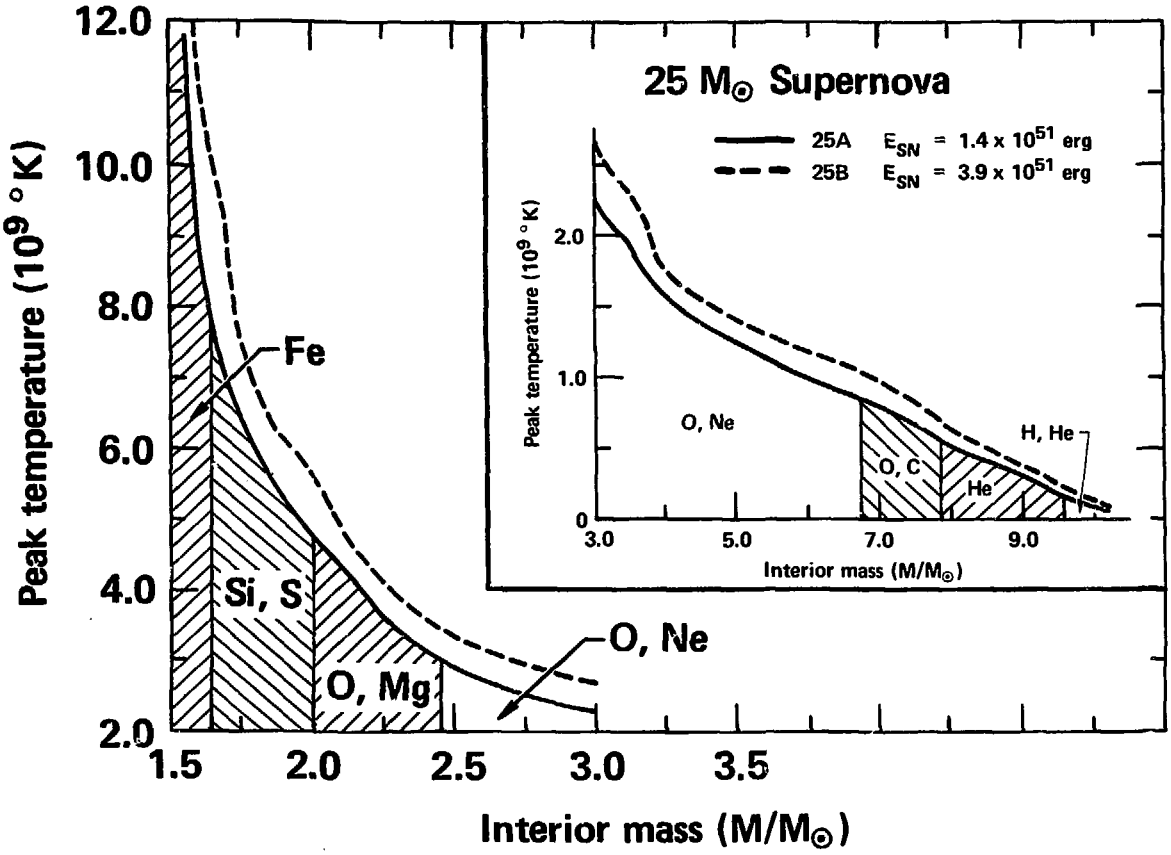
12.0
10.0
8.0
6.0
4.0
2.0
Peak temperature (10^9 °K)
Fe
Si, S
O, Mg
O, Ne
1.5
2.0
2.5
3.0
3.5
Interior mass ($M/M_\odot$)
25 $M_\odot$ Supernova
25A E_{SN} = 1.4 x 10^{51} erg
25B E_{SN} = 3.9 x 10^{51} erg
Peak temperature (10^9 °K)
2.0
1.0
0
O, Ne
O, C
He
H, He
3.0
5.0
7.0
9.0
Interior mass ($M/M_\odot$)

FIGURE 5

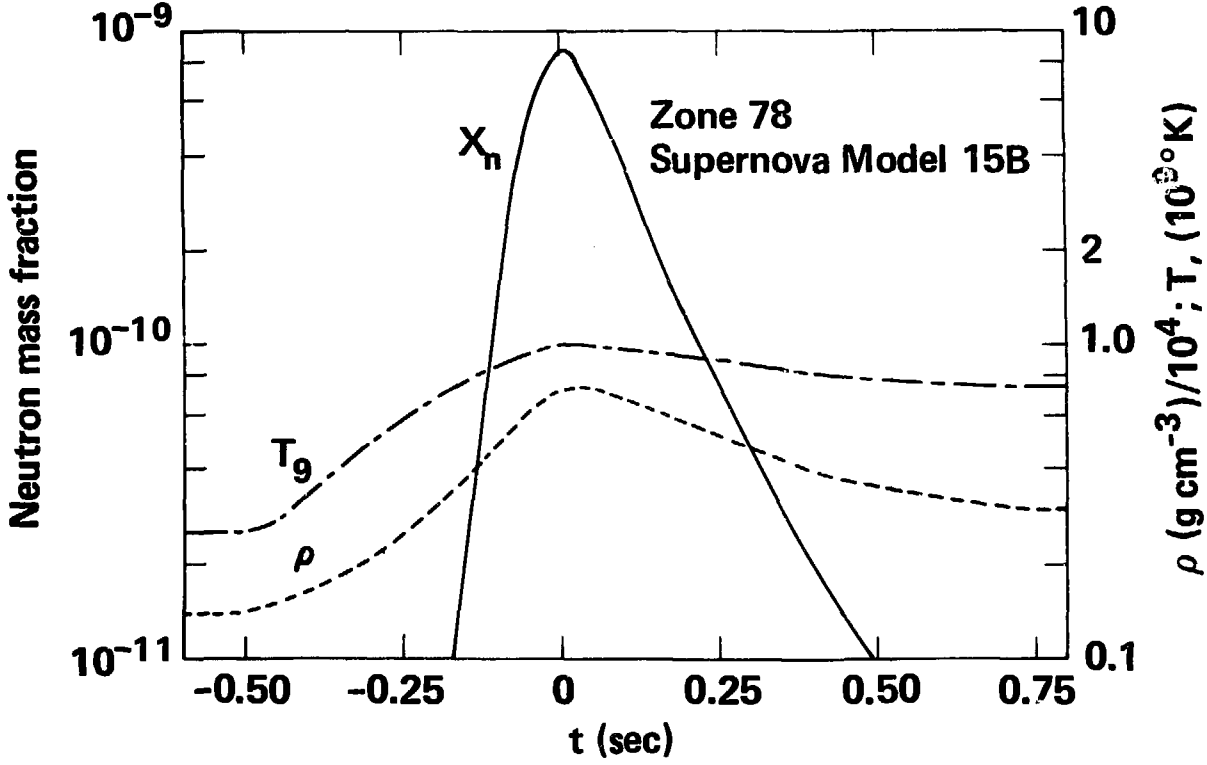
Zone 78
Supernova Model 15B
X_n
T_9
ρ
Neutron mass fraction
10^{-9}
10^{-10}
10^{-11}
10
2
1.0
0.1
ρ (g cm^{-3})/10^4; T, (10^9°K)
-0.50
-0.25
0
0.25
0.50
0.75
t (sec)

FIGURE 6

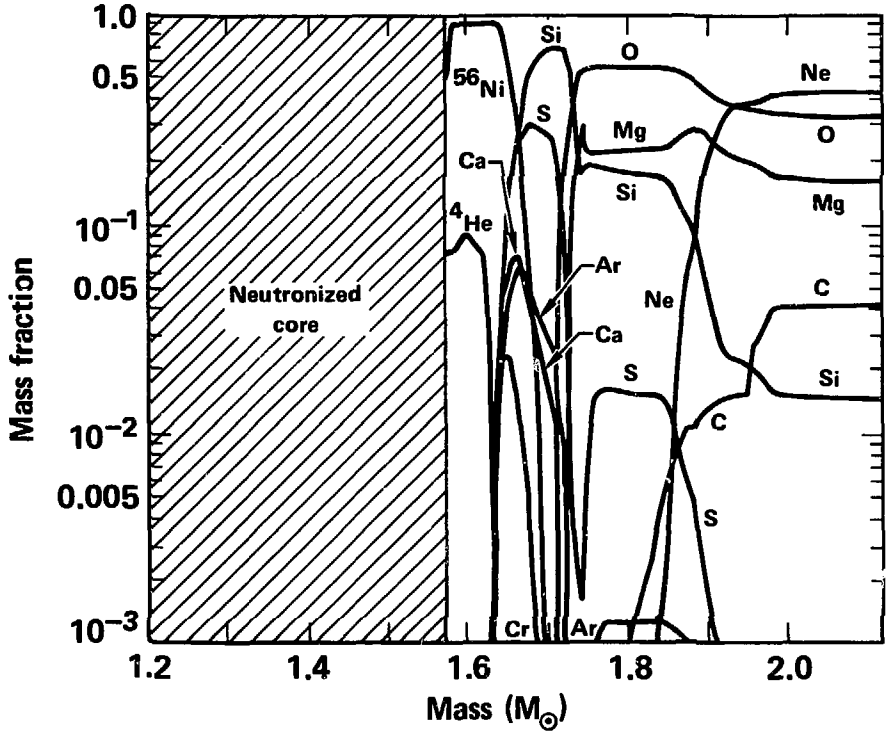
1.0
0.5
10^{-1}
0.05
10^{-2}
0.005
10^{-3}
Mass fraction
Neutronized core
^{56}Ni
^{4}He
Si
S
Ca
Ar
Cr
O
Mg
Ne
C
1.2
1.4
1.6
1.8
2.0
Mass ($M_\odot$)

FIGURE 7a

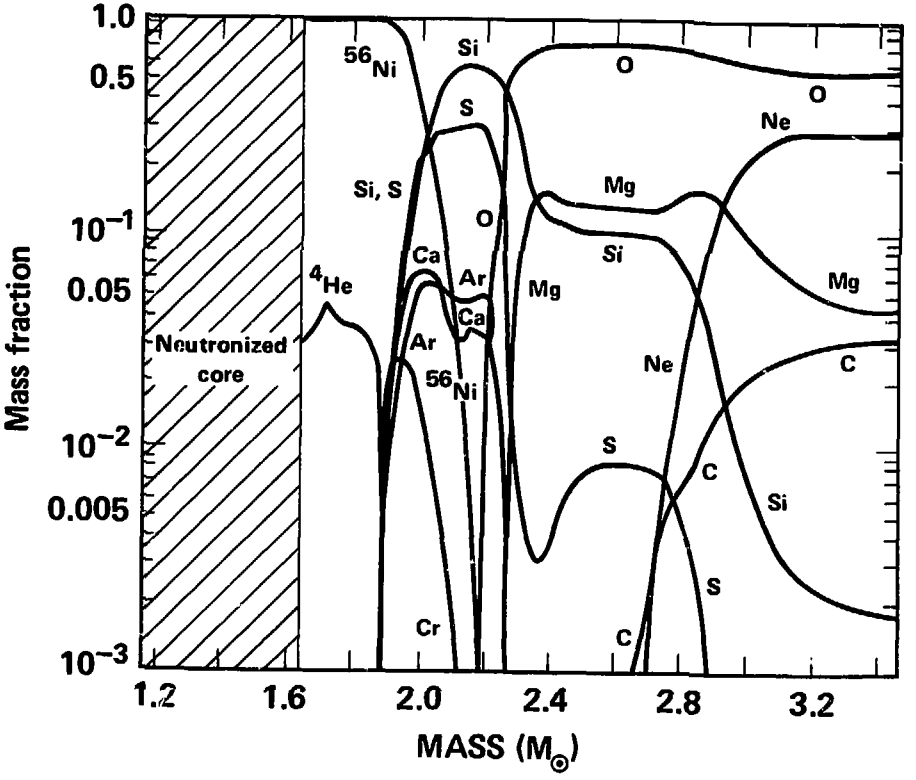
1.0
0.5
10^{-1}
0.05
10^{-2}
0.005
10^{-3}
Mass fraction
1.2
1.6
2.0
2.4
2.8
3.2
MASS ($M_\odot$)
Neutronized core
^{56}Ni
Si
S
Si, S
O
Ca
Ar
^{4}He
Mg
Si
Ca
Ar
^{56}Ni
Cr
S
C
Ne
C
Si
S
C
O
O
Ne
Mg
Mg

FIGURE 7b

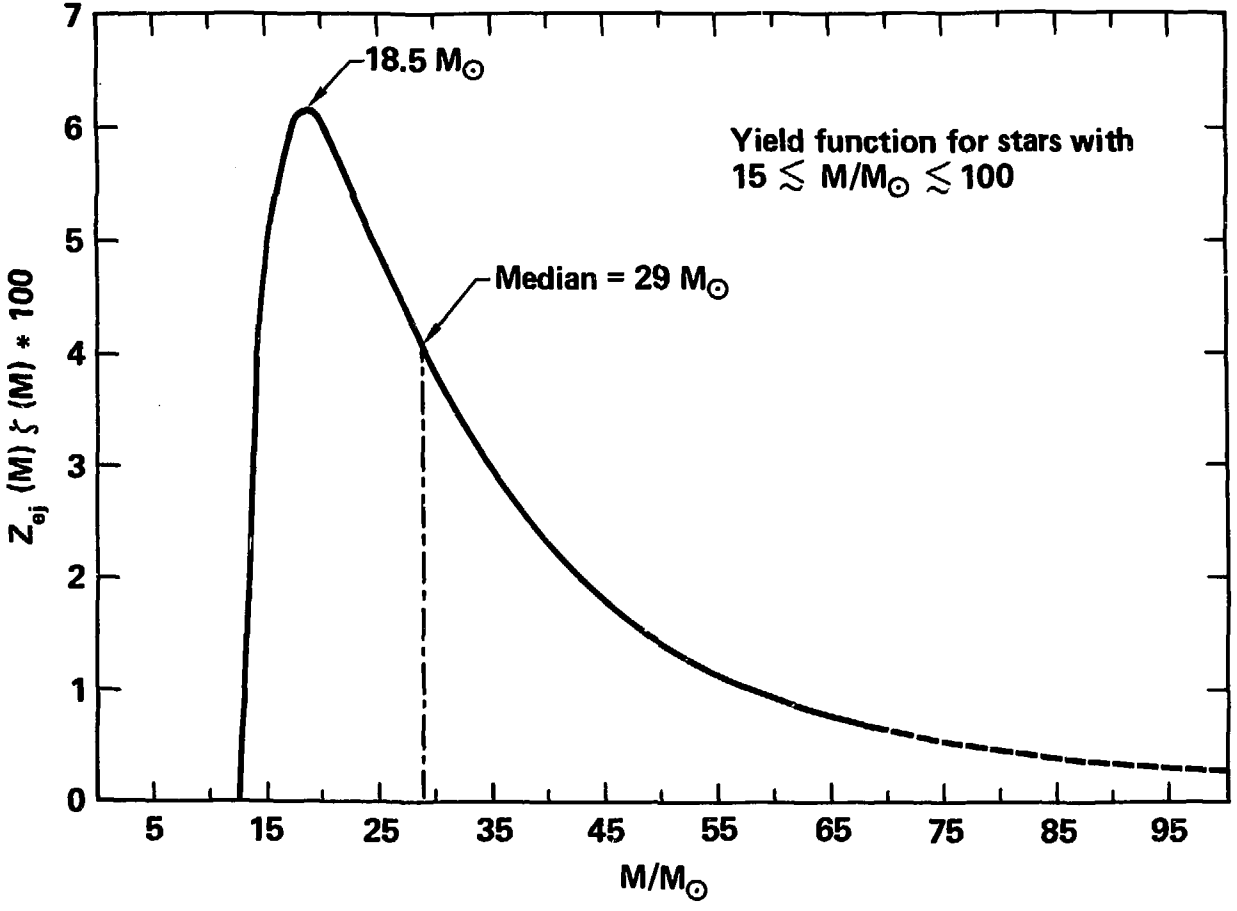
18.5 M⊙
Yield function for stars with
15 ≲ M/M⊙ ≲ 100
Median = 29 M⊙
Z_ej (M) ζ (M) * 100
M/M⊙
0
1
2
3
4
5
6
7
5
15
25
35
45
55
65
75
85
95

FIGURE 8

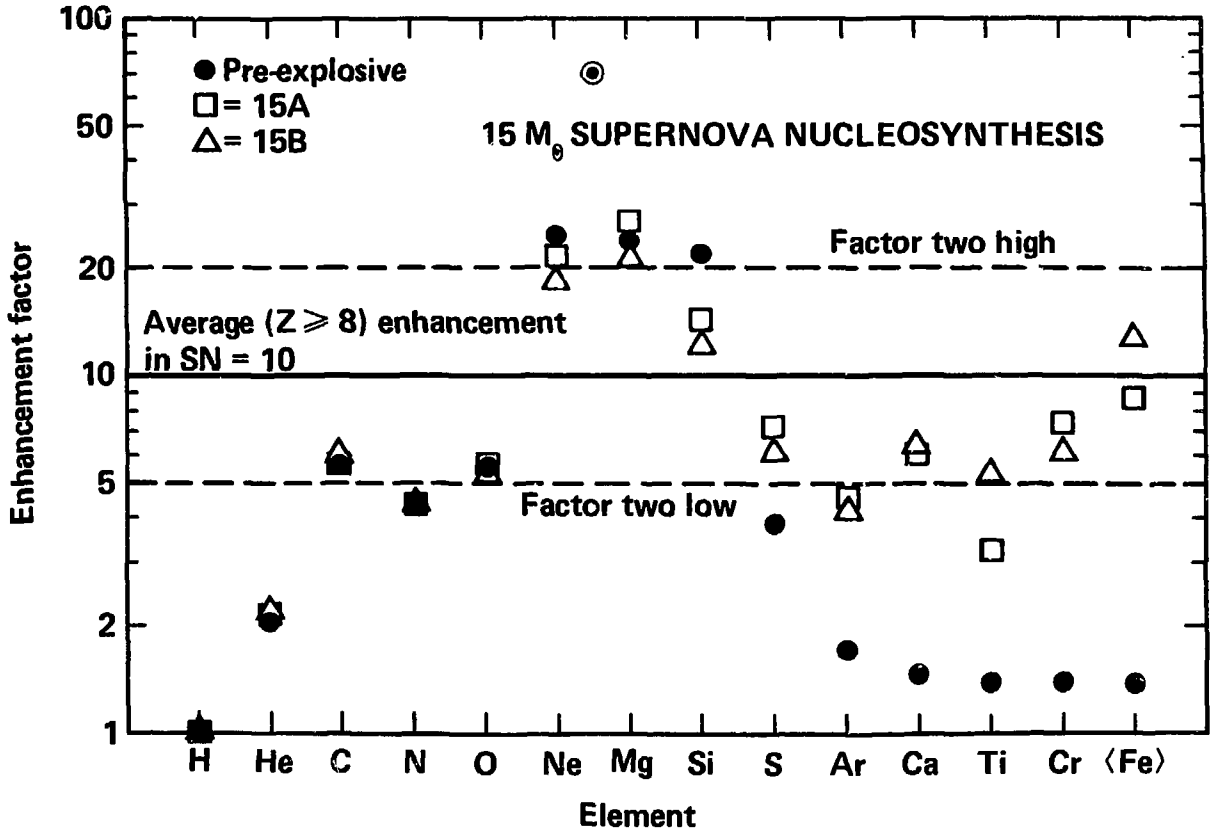
● Pre-explosive
□= 15A
△= 15B
15 M⊙ SUPERNOVA NUCLEOSYNTHESIS
Factor two high
Average (Z ⩾ 8) enhancement in SN = 10
Factor two low
Enhancement factor
100
50
20
10
5
2
1
H
He
C
N
O
Ne
Mg
Si
S
Ar
Ca
Ti
Cr
⟨Fe⟩
Element

FIGURE 9a

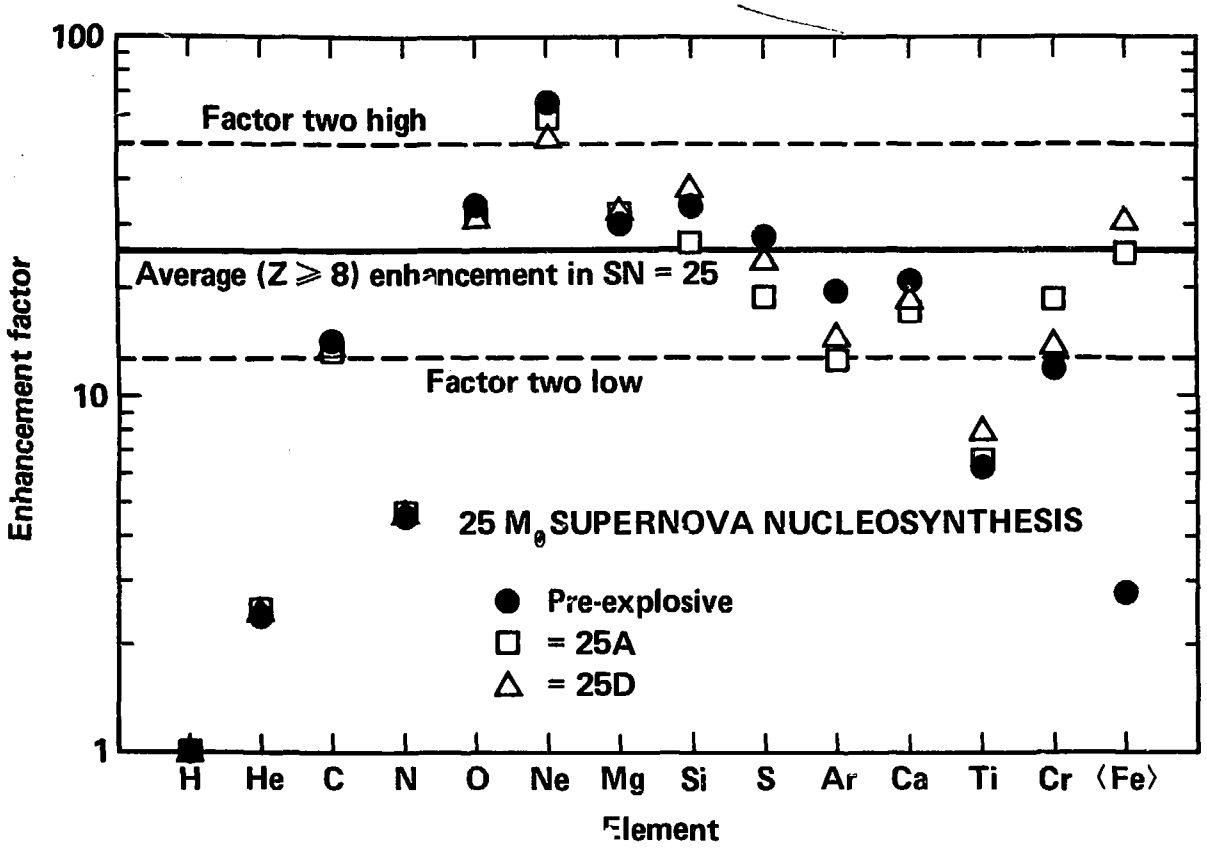
100
10
1
Enhancement factor
Factor two high
Average (Z ⩾ 8) enhancement in SN = 25
Factor two low
25 M⊙ SUPERNOVA NUCLEOSYNTHESIS
Pre-explosive
= 25A
= 25D
H
He
C
N
O
Ne
Mg
Si
S
Ar
Ca
Ti
Cr
⟨Fe⟩
Element

FIGURE 9b

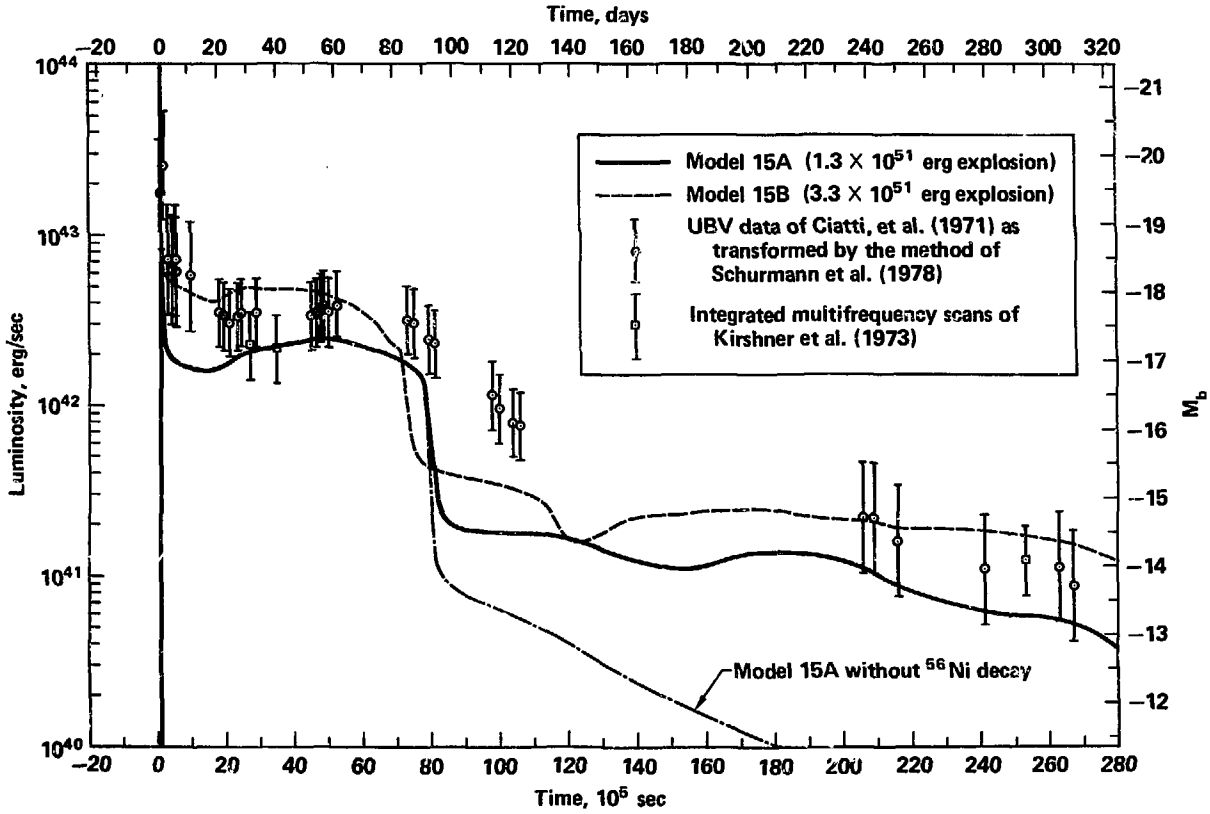
Time, days
−20 0 20 40 60 80 100 120 140 160 180 200 220 240 260 280 300 320
Luminosity, erg/sec
10^{44}
10^{43}
10^{42}
10^{41}
10^{40}
M_b
−21
−20
−19
−18
−17
−16
−15
−14
−13
−12
Model 15A (1.3 X 10^{51} erg explosion)
Model 15B (3.3 X 10^{51} erg explosion)
UBV data of Ciatti, et al. (1971) as transformed by the method of Schurmann et al. (1978)
Integrated multifrequency scans of Kirshner et al. (1973)
Model 15A without ^{56}Ni decay
−20 0 20 40 60 80 100 120 140 160 180 200 220 240 260 280
Time, 10^5 sec

FIGURE 10

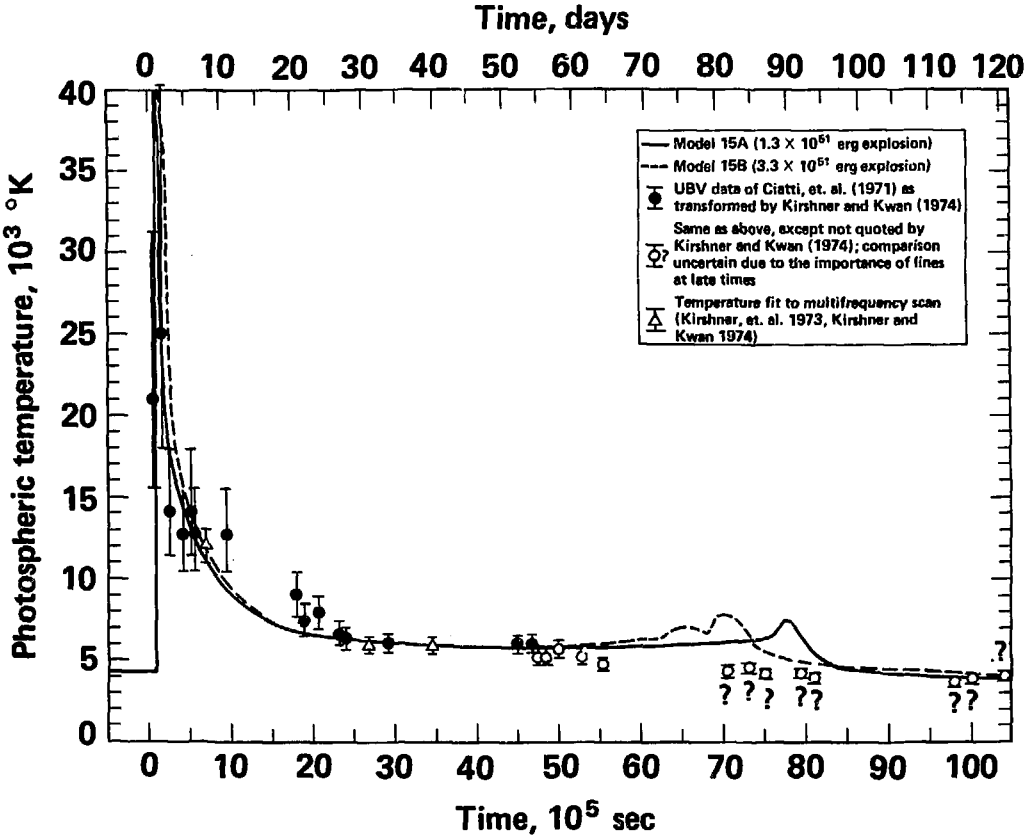
Time, days
0 10 20 30 40 50 60 70 80 90 100 110 120
Photospheric temperature, 10^3 °K
40 35 30 25 20 15 10 5 0
Model 15A (1.3 X 10^{51} erg explosion)
Model 15B (3.3 X 10^{51} erg explosion)
UBV data of Ciatti, et. al. (1971) as transformed by Kirshner and Kwan (1974)
Same as above, except not quoted by Kirshner and Kwan (1974); comparison uncertain due to the importance of lines at late times
Temperature fit to multifrequency scan (Kirshner, et. al. 1973, Kirshner and Kwan 1974)
0 10 20 30 40 50 60 70 80 90 100
Time, 10^5 sec

FIGURE 11

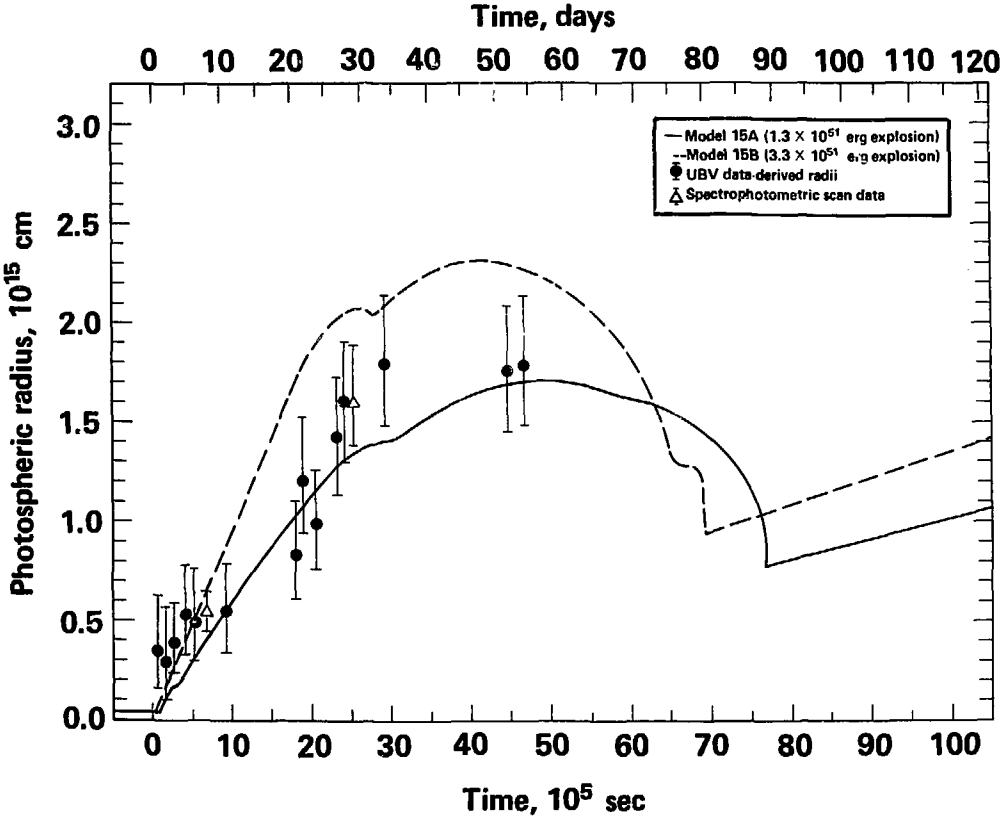
Time, days
0 10 20 30 40 50 60 70 80 90 100 110 120
Photospheric radius, 10^{15} cm
3.0
2.5
2.0
1.5
1.0
0.5
0.0
Model 15A (1.3×10^{51} erg explosion)
Model 15B (3.3×10^{51} erg explosion)
UBV data-derived radii
Spectrophotometric scan data
0 10 20 30 40 50 60 70 80 90 100
Time, 10^5 sec

FIGURE 12

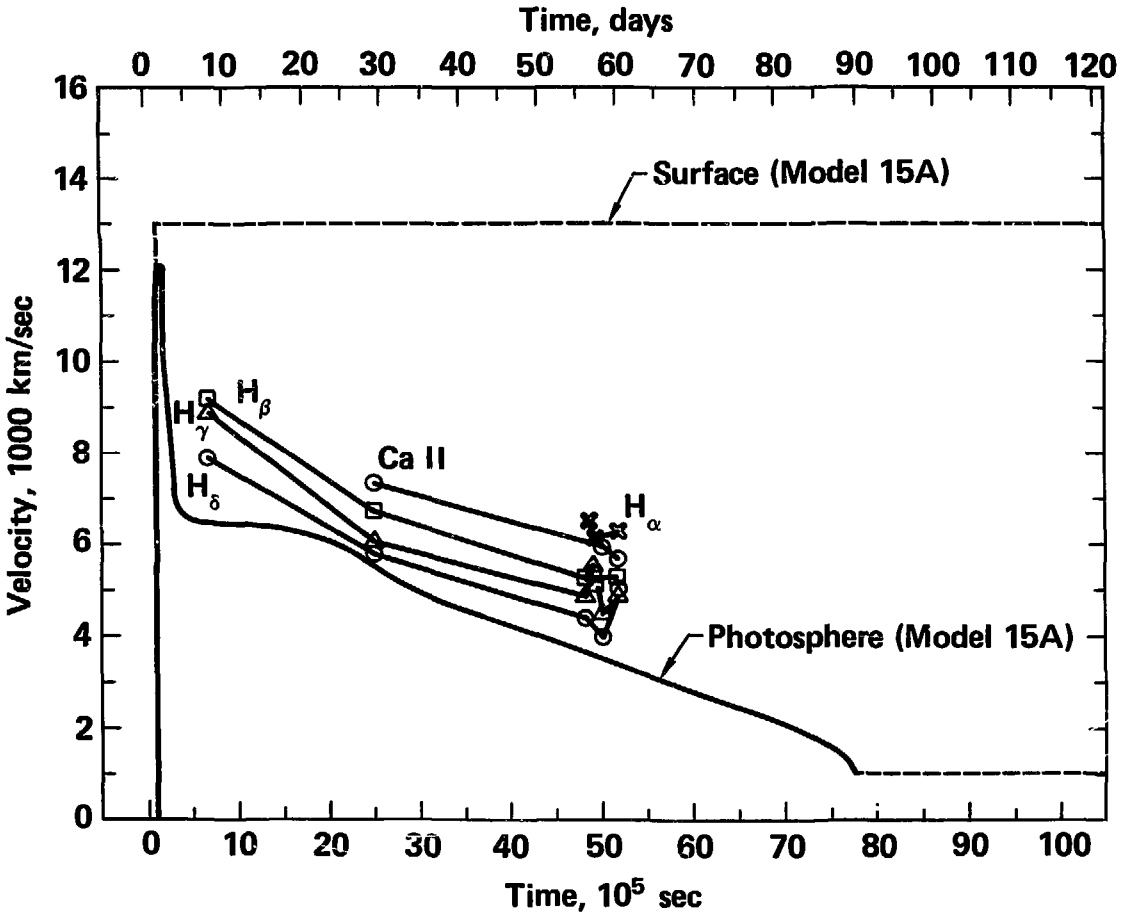
Time, days
0 10 20 30 40 50 60 70 80 90 100 110 120
Surface (Model 15A)
Velocity, 1000 km/sec
16 14 12 10 8 6 4 2 0
H_β
H_γ
H_δ
Ca II
H_α
Photosphere (Model 15A)
0 10 20 30 40 50 60 70 80 90 100
Time, 10^5 sec

FIGURE 13

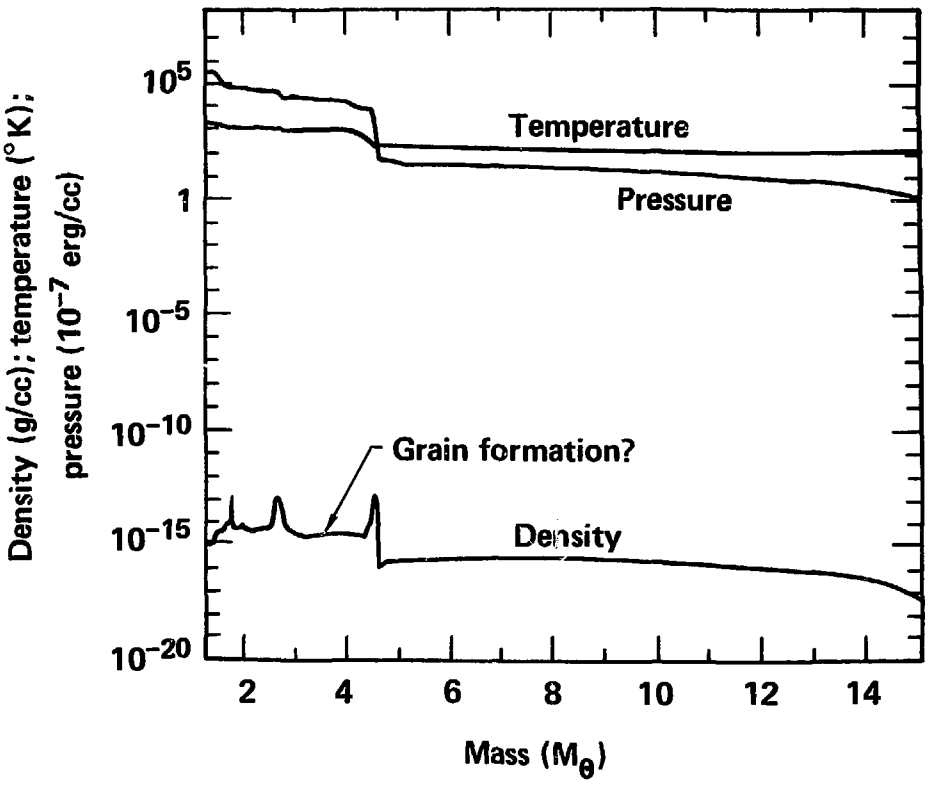
Density (g/cc); temperature (°K); pressure (10^{-7} erg/cc)
10^5
1
10^{-5}
10^{-10}
10^{-15}
10^{-20}
Temperature
Pressure
Grain formation?
Density
2
4
6
8
10
12
14
Mass (M_θ)

FIGURE 14